Inorganic Chemistry

Article

pubs.acs.org/IC

Synthesis of CuTCNQ/Au Microrods by Galvanic Replacement of Semiconducting Phase I CuTCNQ with $KAuBr_4$ in Aqueous Medium

Andrew Pearson, Anthony P. O'Mullane, Suresh K. Bhargava,* and Vipul Bansal*

School of Applied Sciences, RMIT University, GPO Box 2476 V, Melbourne, VIC 3001, Australia

Supporting Information

ABSTRACT: The spontaneous reaction between microrods of an organic semiconductor molecule, copper 7,7,8,8-tetracyanoquinodimethane (CuTCNQ) with $[AuBr_4]^-$ ions in an aqueous environment is reported. The reaction is found to be redox in nature which proceeds via a complex galvanic replacement mechanism, wherein the surface of the CuTCNQ microrods is replaced with metallic gold nanoparticles. Unlike previous reactions reported in acetonitrile, the galvanic replacement reaction in aqueous solution proceeds via an entirely different reaction mechanism, wherein a cyclical reaction mechanism involving continuous regeneration of CuTCNQ consumed during the galvanic replacement reaction occurs in parallel with the galvanic replacement reaction. This results in the driving force of the galvanic replacement reaction in aqueous medium being largely dependent on the availability of $[AuBr_4]^-$ ions during the reaction. Therefore, this study highlights the importance of the choice of an appropriate solvent during galvanic replacement reactions, which can significantly impact upon the reaction mechanism. The reaction progress with respect to different gold salt concentration was monitored using Fourier transform infrared (FT-IR), Raman, and X-ray photoelectron spectroscopy (XPS), as well as XRD and EDX analysis, and SEM imaging. The CuTCNQ/Au nanocomposites were also investigated for their potential photocatalytic properties, wherein the destruction of the organic dye, Congo red, in a simulated solar light environment was found to be largely dependent on the degree of gold nanoparticle surface coverage. The approach reported here opens up new possibilities of decorating metal−organic charge transfer complexes with a host of metals, leading to potentially novel applications in catalysis and sensing.

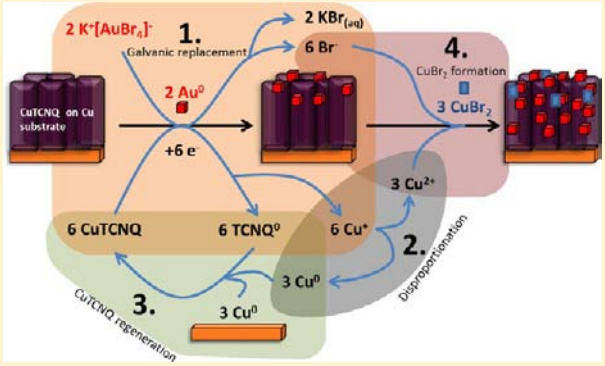

1. INTRODUCTION

Over the past few decades, significant attention has been directed toward metal−organic semiconducting materials based on charge-transfer complexes of metal-7,7,8,8-tetracyanoquinodimethane (TCNQ), principally investigated by Dunbar, Miller, and Bond.[1−13] In particular, CuTCNQ has been the subject of intensive research, based on the observation of switching effects from a high to low impedance state upon application of an external electric field or optical excitation.[14−18] There exists two phases of CuTCNQ, namely phase I, which possesses a higher room-temperature conductivity (0.2 S cm^{-2}), with respect to phase II (1×10^{-5} S cm^{-2}). The two phases also differ in morphology: phase I tends to form rodlike structures and phase II typically leads to platelike structures. For this study, we have employed phase I CuTCNQ, because of the ease of synthesis and advantageous electronic properties, such as improved conductivity, which should make phase I more suited to potential photocatalytic applications. Very recently, we demonstrated that the surface of CuTCNQ structures can be modified using an elegant galvanic replacement approach.[19] This was the first time that galvanic replacement of a semiconducting charge transfer complex with metal ions was reported, thus significantly widening the scope and potential of galvanic replacement reactions for fabricating hybrid nanocomposite materials. Notably, prior to our recent report, the application of CuTCNQ had been limited almost exclusively to switching and field-emission devices;[14,15,17,18,20−24] however, we were also able to demonstrate that CuTCNQ decorated with Au nanoclusters can be appreciably employed as a photocatalytically active substrate for the oxidation of organic dyes, demonstrating that CuTCNQ, when used as a support for metal nanoparticles, can have activity similar to that demonstrated by metal oxides such as TiO_2, SnO_2, WO_3, and ZnO.[25−31]

In a typical galvanic replacement reaction, sacrificial metal templates such as Ag, Co, Ni, and Cu are replaced with more noble metals by reacting the template with noble-metal ions such as $Au^{(III)}$, $Pd^{(IV)}$, and $Pt^{(IV)}$ salts in the absence of any external applied potential, thus creating bimetallic colloids and surfaces.[19,32−35] Depending on reaction parameters such as template morphology,[35,36] reaction medium,[37,38] oxidation state of metal ions,[39−41] etc., the galvanic replacement process can lead to a variety of colloidal materials that can be hollow,

Received: March 14, 2012
Published: August 1, 2012

   dx.doi.org/10.1021/ic300555j | Inorg. Chem. 2012, 51, 8791−8801

dendritic in nature, or highly porous and nanostructured surfaces that are typically decorated with metal nanoparticles.[42−46]

In our previous study, when the galvanic replacement of CuTCNQ with $[AuBr_4]^-$ ions was investigated in acetonitrile, we observed two parallel reaction mechanisms, which were substrate-independent and involved the galvanic replacement of CuTCNQ to form metallic Au from $[AuBr_4]^-$ that competed with the dissolution of CuTCNQ into acetonitrile.[19] In this current study, we have extended our previous work and explored the significant effect that an aqueous solvent can have on the galvanic replacement of CuTCNQ with $[AuBr_4]^-$ ions. The current study demonstrates that, because of the difference in solubility of the precursors and reaction intermediates, and the involvement of the Cu substrate on which CuTCNQ crystals are grown, the galvanic replacement reaction between CuTCNQ microrods and $AuBr_4^-$ ions in aqueous solution follows a dramatically different pathway than that previously observed in acetonitrile. This study also shows that the surface coverage of the CuTCNQ microrods with Au nanoclusters can be appreciably fine-tuned by controlling the concentration of $[AuBr_4]^-$ ions during galvanic replacement process. Furthermore, photocatalysis being recently discovered as a relatively new application of CuTCNQ-based materials,[19] the CuTCNQ/Au nanocomposites obtained in aqueous medium were investigated for the photocatalytic degradation of a model organic azo dye Congo red.

2. METHODOLOGY

2.1. Materials. Copper metal foil (99% purity) was obtained from Chem Supply; 7,7,8,8-tetracyanoquinodimethane (TCNQ) was obtained from Fluka; potassium tetrabromoaurate ($KAuBr_4{\cdot}3H_2O$) and Congo red were obtained from Sigma−Aldrich; and acetonitrile was obtained from BDH Chemicals. Copper foil was treated with dilute nitric acid, rinsed with water, and dried with a flow of nitrogen immediately before use. All other chemicals were used as received.

2.2. Phase I CuTCNQ Synthesis in Acetonitrile. A 15 cm × 1.5 cm × 0.015 cm strip of copper foil was first immersed in dilute nitric acid to facilitate the removal of any oxide species on the copper surface. The copper foil was then washed with deionized water and immediately placed in 50 mL of 5 mM TCNQ solution in acetonitrile. The surface of the copper foil was observed to turn black in color with a dark bluish/purplish tinge, indicating the formation of CuTCNQ. The reaction was allowed to proceed for 1 h. The CuTCNQ foil was then washed three times with deionized water and dried under nitrogen. After the CuTCNQ foil was sufficiently washed and dried, the 15 cm × 1.5 cm piece of foil was cut into ten 1.5 cm × 1.5 cm pieces to ensure that all subsequent experiments were performed on the same batch of CuTCNQ.

2.3. Galvanic Replacement of CuTCNQ with $KAuBr_4$ in Water. Eight 1.5 cm × 1.5 cm pieces of CuTCNQ synthesized in acetonitrile were each added to separate solutions containing increasing concentrations (1 μM, 10 μM, 50 μM, 100 μM, 500 μM, 1 mM, 10 mM, and 100 mM) of $KAuBr_4$ in 5 mL of deionized water. The galvanic replacement reaction between CuTCNQ and $KAuBr_4$ was then allowed to proceed for 4 h. After 4 h, the pieces of CuTCNQ were removed from solution and washed three times with deionized water to remove any residual reactants and soluble products. The galvanically replaced CuTCNQ substrates were examined without any further modification using scanning electron microscopy (FEI NovaSEM), electron-dispersive X-rays (EDX performed on FEI NovaSEM instrument coupled with EDX Si(Li) X-ray detector), X-ray photoelectron spectroscopy (Thermo K-Alpha XPS instrument at a pressure better than 1×10^{-9} Torr with core levels aligned with a C 1s binding energy of 285 eV), X-ray diffraction (XRD, Bruker Model AXS D8 Discover with General Area Detector Diffraction System), Fourier transform infrared spectroscopy (FT-IR, Perkin−Elmer Spectrum 100), and Raman spectroscopy (Perkin−Elmer Raman Station 200F). In a control experiment, to observe the effect of copper foil on galvanic replacement reaction, the CuTCNQ crystals grown onto copper foil in acetonitrile were separated by scratching the surface, followed by galvanic replacement of 1 mg of CuTCNQ powders (in the absence of Cu foil) with increasing concentrations (1 μM, 10 μM, 50 μM, 100 μM, 500 μM, 1 mM, 10 mM, and 100 mM) of $KAuBr_4$ in 5 mL of deionized water for 4 h.

2.4. Photocatalytic Experiments. The photocatalytic activity of the galvanically replaced phase I CuTCNQ substrates was examined by immersing a 1.5 cm × 1.5 cm piece of CuTCNQ in a 5-mL, 50-μM aqueous solution of the organic dye "Congo red" (CR) and recording the intensity of the characteristic absorption maxima at ca. 500 nm after exposure to simulated solar light (based on equatorial conditions) for a period of 30 min. An Abet Technologies LS-150 Series 150W Xe arc lamp source with a condensing lens was used with the sample placed in a quartz vial at the distance of 7 cm from the source with slow mechanical stirring to promote mixing of the solution. After 30 min of irradiation, the composite was removed by centrifugation and the remaining solution was examined by UV−vis spectroscopy.

3. RESULTS AND DISCUSSION

Illustrated in Figure 1 are representative SEM images of phase I CuTCNQ microrods that have been synthesized through

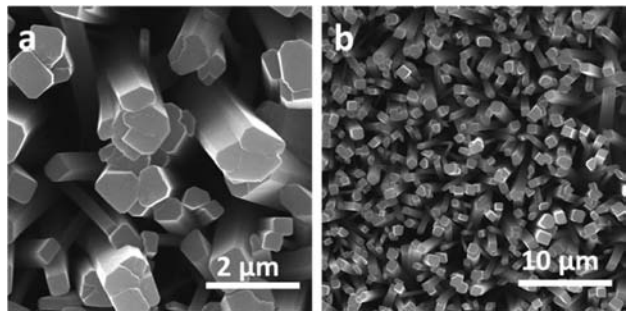

Figure 1. SEM images of pristine CuTCNQ microrods synthesized in acetonitrile on a Cu foil.

reaction between copper foil and a solution of 5 mM TCNQ in acetonitrile, as reported in our previous work.[19] A dense coverage of CuTCNQ microrods with an average cross section of 1 μm × 1 μm with faceted corners and lengths on the order of 10−20 μm can be clearly observed (Figure 1). Since these CuTCNQ microrods were formed by immersion of a Cu foil in TCNQ solution, it should be noted that uniform coverage of CuTCNQ microrods was observed on both the sides of Cu foil (as confirmed by SEM—data not shown for brevity). EDX analysis shows signals corresponding to C, N, O, and Cu, arising from these microrods, suggesting that the structures formed are CuTCNQ crystals (see Figure 3, presented later in this paper). FT-IR spectroscopic analysis further confirms that the microrods are indeed phase I CuTCNQ, demonstrating characteristic vibration modes at 2199, 2171, and 825 cm^{-1} (Figure 4a, presented later in this paper).[1]

In our previous work, we demonstrated the reaction of phase I CuTCNQ microrods with different concentrations of $[AuBr_4]^-$ ions in acetonitrile[19] and confirmed that two competing reaction mechanisms occur during galvanic replacement in acetonitrile. Because of the partial solubility of CuTCNQ in acetonitrile (0.14 ± 0.04 mM), under conditions of low gold salt concentration, the dissolution of CuTCNQ is the dominant process and results in the formation of hollow CuTCNQ rods via: $CuTCNQ_{(s)} \rightarrow Cu^+ + TCNQ^-$. As the

dx.doi.org/10.1021/ic300555j | Inorg. Chem. 2012, 51, 8791−8801

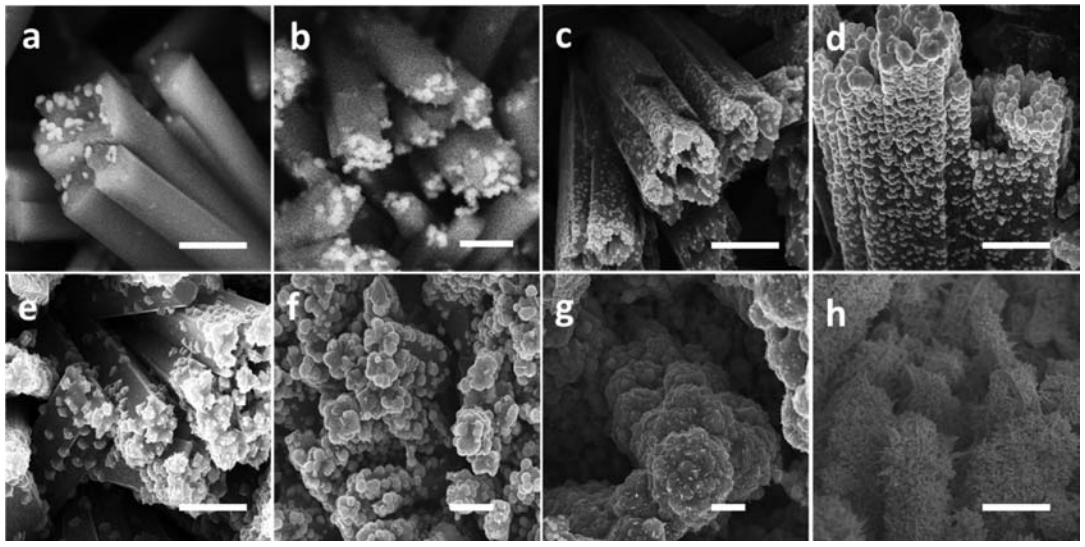

Figure 2. SEM images of CuTCNQ microrods galvanically replaced with (a) 1 μM, (b) 10 μM, (c) 50 μM, (d) 100 μM, (e) 500 μM, (f) 1 mM, (g) 10 mM, and (h) 100 mM $[AuBr_4]^-$ ions in aqueous solution. Scale bars correspond to 1 μm in (panels a–g) and 5 μm in panel (h).

gold salt concentration is increased, this dissolution process becomes more inhibited as the redox reaction between phase I CuTCNQ and $[AuBr_4]^-$ ions takes effect, which results in extensive coverage of CuTCNQ with metallic Au with an evidence of surface confined neutral TCNQ formation that is inaccessible to the acetonitrile solution via: 3CuTCNQ + $KAuBr_4 \rightarrow Au^0 + 3TCNQ^0 + 3CuBr + KBr$.[19] In contrast to our previous work, galvanic replacement of the CuTCNQ microrods was investigated in aqueous solution in the current study. CuTCNQ is not appreciably soluble in water, which was confirmed by immersing CuTCNQ in water where no structural change in CuTCNQ crystals was observed even after several weeks of immersion (SEM images are not shown for the sake of brevity). Galvanic replacement of CuTCNQ microrods with 1 μM $[AuBr_4]^-$ ions (Figure 2a) results in the decoration of irregularly shaped sub-100 nm Au clusters on the topmost faces of the CuTCNQ rods. As expected, unlike our previous work in acetonitrile solution wherein CuTCNQ rods became hollow,[19] no dissolution of CuTCNQ is observed during galvanic replacement in water and the CuTCNQ rods remain intact. However, in water, even at 1 μM $[AuBr_4]^-$ concentration, decoration of Au nanoparticles on the top faces of CuTCNQ rods was observed, which was conversely not observed previously during galvanic replacement with such low gold salt concentrations in acetonitrile. Higher magnification images corresponding to reaction of CuTCNQ microrods with different concentrations of $[AuBr_4]^-$ ions are displayed in Supporting Information in Figure S1.

By increasing the $[AuBr_4]^-$ ions concentration to 10 μM (Figure 2b), deposition of irregularly shaped sub-100 nm nanoparticles, along with smaller sub-10 nm Au nanoparticles, is observed to occur on the CuTCNQ microrods. Increasing the concentration of $[AuBr_4]^-$ ions to 50 μM (Figure 2c) results in the deposition of a larger number of sub-100 nm quasi-spherical Au nanoparticles. Interestingly, these nanoparticles are now observed to decorate the sides of the rods with the number of Au nanoparticles becoming sparser further along the rods toward the Cu substrate. Further increasing the $[AuBr_4]^-$ ions concentration to 100 μM (Figure 2d) results in Au nanoparticle decoration similar to that observed for 50 μM $[AuBr_4]^-$ ions, however with an increase in the density of Au nanoparticles loading. Interestingly, unlike the trend observed up to 100 μM gold salt concentrations, further increasing the concentration to 500 μM (Figure 2e) does not lead to an increase in the number of Au nanoparticles decorating the CuTCNQ surface, rather the Au nanoparticles seem to undergo an interesting morphology change toward becoming cubic with well-defined edges ca. 200 nm in length (as can be observed clearly in higher magnification SEM images shown in Figure S1e in the Supporting Information). Similarly, reaction with 1 mM $[AuBr_4]^-$ ions (Figure 2f) results in the decoration of larger (200–300 nm) Au clusters that, at higher magnification, appear to be agglomerates of many smaller cubic nanocrystals (see Figure S1f in the Supporting Information). At this stage of Au cluster decoration, almost the entire CuTCNQ rod is covered with Au clusters to the extent where little of the CuTCNQ rod can be observed.

By greatly increasing the $[AuBr_4]^-$ concentration to 10 mM (Figure 2g), complete coverage of the CuTCNQ rods with a thick covering of large Au clusters, which range in size from 200 nm to 1000 nm can be achieved. Once again, at higher magnification, these also appear to be large agglomerates of cubic crystals (see Figure S1g in the Supporting Information). Interestingly, at this higher gold salt concentration, small platelike crystals ranging in size from 100 nm to 200 nm are observed decorating the Au layer over the CuTCNQ surface, which were confirmed by EDX and XRD to be consisted of $CuBr_2$. Finally, increasing the concentration of $[AuBr_4]^-$ ions to 100 mM (Figure 2h) results in even denser coverage of the CuTCNQ rods with a needlelike Au growth. Higher-magnification SEM images further established that this Au needlelike surface was covered with large 2–3 μM flat cubic crystals of $CuBr_2$ (Figure S1h in the Supporting Information).

The formation of Au clusters on the surface of the CuTCNQ microrods was followed using EDX analysis, wherein a continuous increase in the signature corresponding to the Au Mα and Mβ lines is observed with increasing $[AuBr_4]^-$ ions concentration during galvanic replacement with CuTCNQ (Figure 3). Characteristic energy lines corresponding to C Kα, N Kα, O Kα, and Cu Lα are observed in all samples at 0.277, 0.392, 0.524, and 0.929 keV, respectively. As the concentration of $[AuBr_4]^-$ ions is increased, a peak correlating to the Au Mα

dx.doi.org/10.1021/ic300555j | Inorg. Chem. 2012, 51, 8791–8801

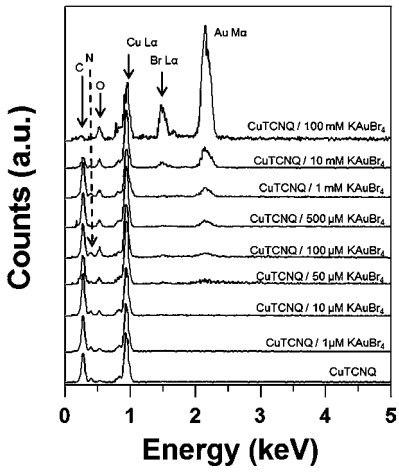

Figure 3. EDX analysis of CuTCNQ microrods before and after their galvanic replacement with increasing concentrations of $[AuBr_4]^-$ ions. All the spectra have been normalized in intensity to Cu Lα signal, and corresponding C Kα, N Kα, O Kα, Br Lα, Cu Lα, and Au Mα/Au Mβ energy levels are labeled.

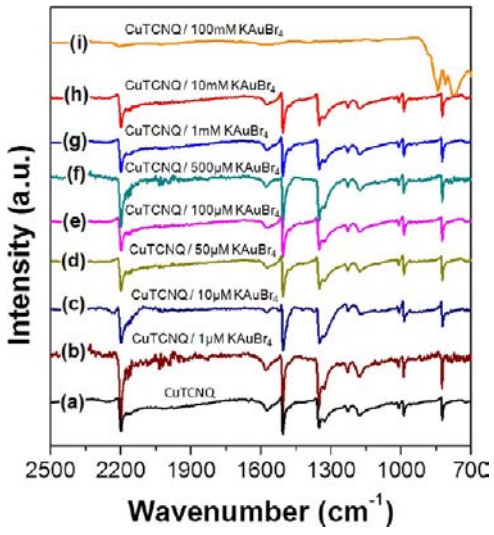

Figure 4. FT-IR spectra of CuTCNQ microrods before reaction (spectrum a) and after reaction with 1 μM (spectrum b), 10 μM (spectrum c), 50 μM (spectrum d), 100 μM (spectrum e), 500 μM (spectrum f), 1 mM (spectrum g), 10 mM (spectrum h), and 100 mM $[AuBr_4]^-$ ions (spectrum i).

and Mβ lines at 2.122 keV is observed to gradually increase in intensity, indicating an increase in the amount of Au present on the surface of the CuTCNQ rods. Notably, as the concentration of $[AuBr_4]^-$ ions is increased to relatively high concentrations of 10 mM and 100 mM, a strong signature corresponding to the Br Lα is also observed at 1.596 keV, confirming the presence of a Br-containing species that is deposited on the surface of the CuTCNQ microrods during galvanic replacement with higher concentrations of $[AuBr_4]^-$ ions. It is also notable that, at higher $[AuBr_4]^-$ ions concentrations of 10 mM and 100 mM, the C signature arising from CuTCNQ crystals reduces significantly in intensity, which correlates well with the SEM results, wherein at these concentrations, complete coverage of CuTCNQ microrods with Au nanoparticles was observed.

In addition to EDX, FT-IR spectroscopy was performed to obtain additional information regarding the phase structure of CuTCNQ after galvanic replacement with varying concentrations of $[AuBr_4]^-$ ions (Figure 4). FT-IR spectral analysis showed the presence of only phase I CuTCNQ, thus confirming that the phase of pristine CuTCNQ does not change as a result of galvanic replacement with gold salt. This is evident from characteristic FT-IR signatures of synthesized pristine phase I CuTCNQ at ca. 2199, 2171, and 825 cm^{-1}, which do not shift in their positions during reaction with increasing concentrations of $[AuBr_4]^-$ ions, confirming that galvanic replacement reaction does not lead to conversion of phase I CuTCNQ to the phase II material. However, the galvanic replacement of CuTCNQ with the highest 100 mM $[AuBr_4]^-$ ion concentration results in an almost featureless FT-IR spectrum, which could not be attributed to CuTCNQ, implying that a very thick coating of gold on CuTCNQ microrods (as is observed by SEM in Figure 2h and through EDX in Figure 3) inhibits the ability of the FT-IR instrument to collect information on the underlying CuTCNQ.

The galvanic replacement reaction was further examined using X-ray photoelectron spectroscopy (XPS), which is a highly surface sensitive technique and can provide crucial information about the chemical species present in the system.[47] Cu 2p and Au 4f core levels obtained on CuTCNQ samples galvanically replaced with 1 mM and 100 mM $[AuBr_4]^-$ ions are shown in Figure 5. The Cu 2p core levels in the 1 mM $[AuBr_4]^-$ ions (Figure 5a) sample showed two characteristic $2p_{3/2}$ and $2p_{1/2}$ splitting components at 933.7 and 953.7 eV binding energies (BEs), respectively, which can be confidently attributed to phase I CuTCNQ.[24] Significantly, no signature corresponding to shakeup satellite peaks due to the formation of Cu^{2+} is observed, which suggests that the final products of the galvanic replacement reaction with 1 mM $[AuBr_4]^-$ ions remain as Cu^+ (in CuTCNQ).[19,24] However, upon galvanic replacement with 100 mM $[AuBr_4]^-$ ions, a significant shift in the Cu $2p_{3/2}$ BE to ca. 932.6 eV is observed, which is ca. 1.1 eV lower than that observed for galvanic replacement with 1 mM $[AuBr_4]^-$ ions (Figure 5a). The presence of lower BE Cu 2p component in addition to significant shakeup satellite peaks observed in this sample can be attributed to the presence of Cu^{2+} species. Therefore XPS analysis further supports the formation of large $CuBr_2$ crystals during galvanic replacement with high concentration of gold salt, as observed during SEM analysis (Figure 2h and Figure S1h in the Supporting Information), and later confirmed by XRD.[45,48] The Au 4f core levels from CuTCNQ/Au composites obtained using both 1 mM and 100 mM $[AuBr_4]^-$ ions could be split into two characteristic $4f_{7/2}$ and $4f_{5/2}$ components, with $4f_{7/2}$ BE at ca. 84.7 eV (Figure 5b), which is a clear indication of the formation of Au^0,[49] therefore confirming the formation of metallic Au particles during the galvanic replacement reaction.

A powerful tool allowing researchers to probe the differences between the chemical nature of TCNQ species (i.e., $TCNQ^-$ and $TCNQ^0$) in a material is Raman spectroscopy. Displayed in Figure 6 are Raman spectra of pristine TCNQ crystals and CuTCNQ microrods galvanically replaced with increasing concentrations of $[AuBr_4]^-$ ions. CuTCNQ shows four characteristic features in a Raman spectrum principally located at ca. 1200 cm^{-1} (C═CH bending), 1380 cm^{-1} (C−CN wing stretching), 1600 cm^{-1} (C═C ring stretching), and 2200 cm^{-1} (C−N stretching). The only notable difference in the Raman spectra of CuTCNQ/Au nanocomposites with different $[AuBr_4]^-$ ion concentrations is the reduction in the intensity of the major peaks associated with CuTCNQ with increasing

dx.doi.org/10.1021/ic300555j | Inorg. Chem. 2012, 51, 8791−8801

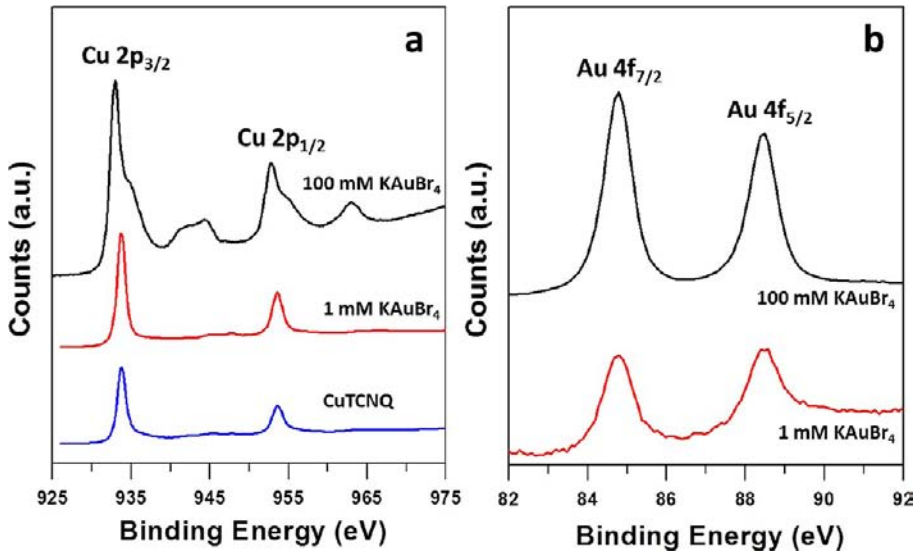

Figure 5. XPS analysis showing the (a) Cu 2p and (b) Au 4f core level spectra from CuTCNQ microrods before and after their reaction with 1 mM and 100 mM $[AuBr_4]^-$ ions in aqueous solution.

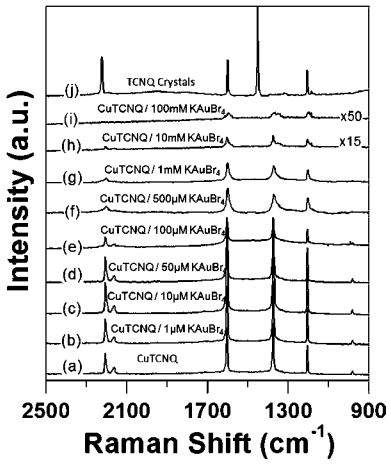

Figure 6. Raman spectra of CuTCNQ microrods before reaction (spectrum a) and after reaction with 1 μM (spectrum b), 10 μM (spectrum c), 50 μM (spectrum d), 100 μM (spectrum e), 500 μM (spectrum f), 1 mM (spectrum g), 10 mM (intensity multiplied 15×) (spectrum h), and 100 mM (intensity multiplied 50×) $[AuBr_4]^-$ ions (spectrum i). Raman spectrum of pristine TCNQ crystals (spectrum j) is also provided for comparison.

concentrations of $[AuBr_4]^-$ ions (spectra a–i in Figure 6). For instance, galvanic replacement with 10 and 100 mM $[AuBr_4]^-$ ions results in almost-complete quenching of the Raman signal attributable to CuTCNQ, whereby the intensity of the Raman spectra required an enhancement by a factor of 15 and 50 (for galvanic replacement with 10 and 100 mM $[AuBr_4]^-$ ions, respectively) for peaks to become discernible. This quenching of the CuTCNQ signatures can be attributed to the thick layer of Au deposited on the surface of the CuTCNQ microrods, essentially preventing Raman interactions. Interestingly, in contrast to our previous study in acetonitrile, galvanic replacement of CuTCNQ with increasing concentrations of $[AuBr_4]^-$ ions does not result in the shift of C–CN wing stretching vibrational mode at 1380 cm^{-1} to ca. 1450 cm^{-1}, which would have otherwise indicated the formation of $TCNQ^0$.[19,50] This provides a strong indication that (i) $TCNQ^0$ is not a product of the galvanic replacement reaction in water and (ii) reaction mechanisms in acetonitrile and water are completely different. It is also noteworthy to add that FT-IR spectra also do not provide any indication of the formation of $TCNQ^0$ (Figure 4).

To further support the results obtained from spectroscopic analysis (Figures 4–6) and to ensure the formation of metallic Au^0 during the galvanic replacement reactions, XRD analysis of CuTCNQ reacted with different concentrations of $[AuBr_4]^-$ ions was performed (Figure 7). Depicted in pattern (a) is the XRD pattern arising from pristine TCNQ powder displaying major peaks at 18.6°, 24.2°, 26.0°, 27.5°, 28.5°, and 30.1° 2θ, which correspond well with the literature for monoclinic TCNQ (JCPDS File Card 00-033-1899). The unmodified CuTCNQ substrate (pattern b) shows XRD signatures at 16.0° and 18.0° 2θ, which can be attributed to phase I CuTCNQ

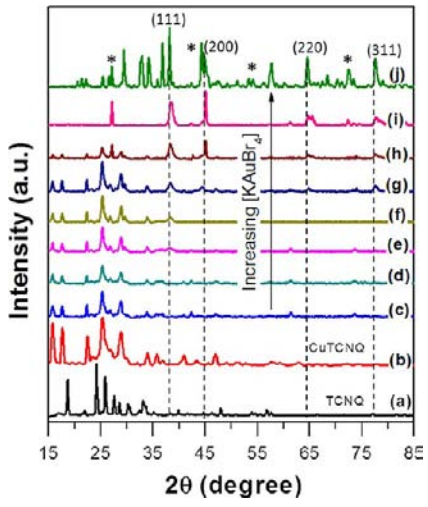

Figure 7. XRD patterns of pristine TCNQ crystals (spectrum a) and CuTCNQ microrods (spectrum b) before galvanic replacement and after galvanic replacement with 1 μM (spectrum c), 10 μM (spectrum d), 50 μM (spectrum e), 100 μM (spectrum f), 500 μM (spectrum g), 1 mM (spectrum h), 10 mM (spectrum i), and 100 mM $[AuBr_4]^-$ ions (spectrum j). Peaks corresponding to fcc gold planes have been labeled. (*) corresponds to signals arising from $CuBr_2$.

dx.doi.org/10.1021/ic300555j | Inorg. Chem. 2012, 51, 8791–8801

Scheme 1. Schematic Representation of the Galvanic Replacement Reaction between CuTCNQ Microrods Grown on an Underlying Cu Substrate and $[AuBr_4]^-$ Ions in an Aqueous Environment[a]

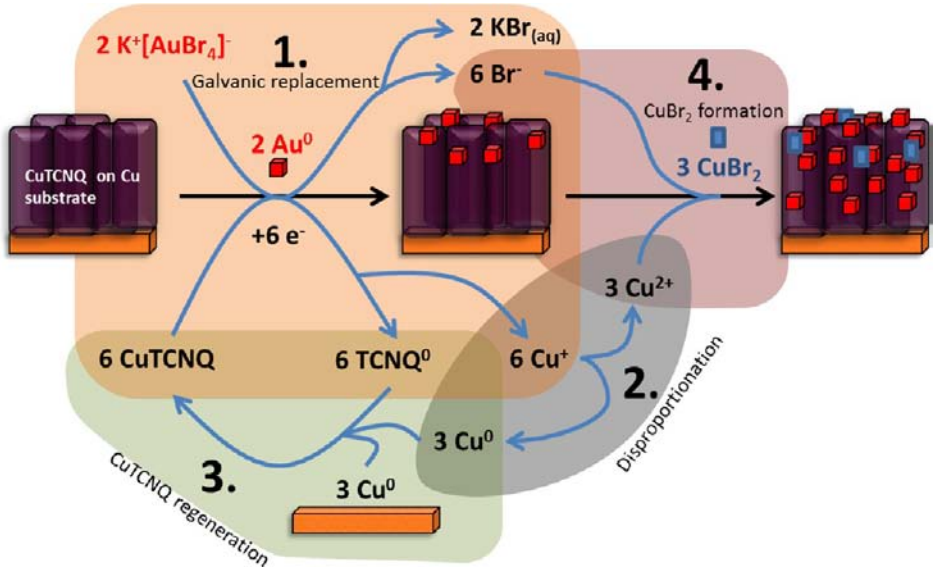

[a]Step 1 involves the galvanic replacement of CuTCNQ by $[AuBr_4]^-$ ions to generate metallic Au^0 by oxidizing CuTCNQ to Cu^+ and $TCNQ^0$, followed by the disproportionation of Cu^+ ions in water to form Cu^0 and Cu^{2+} (Step 2). Step 3 involves the regeneration of CuTCNQ through reaction between the newly generated Cu^0 or that from underlying Cu foil substrate and the $TCNQ^0$ formed by oxidation of CuTCNQ. Finally, step 4 illustrates the formation of $CuBr_2$ from residual Cu^{2+} and Br^- ions.

(JCPDS File Card 00-054-1997), while in addition to these peaks, features at 22.5°, 25.0°, and 29.0° 2θ can also be attributed to CuTCNQ that corroborate well with the literature.[1] Upon reaction with 1 μM and 10 μM $[AuBr_4]^-$ ions (patterns c and d, respectively), insignificant change in the intensity or location of any peaks is observed, which corroborates well with the SEM images (Figures 2a and b, respectively), which show limited decoration of CuTCNQ with Au clusters. The first signatures attributable to the (111) plane of fcc Au (JCPDS File Card 03-065-2870) appear at 38.0° 2θ[51] after galvanic replacement with 50 μM $[AuBr_4]^-$ ions (pattern e), which correlates well with the decoration of CuTCNQ with relatively larger number of Au nanoparticles (Figure 2c). The Au (111) peak further increases in intensity with a further increase in the $[AuBr_4]^-$ ion concentration to 100 μM (pattern f). A further increase in the concentration of $[AuBr_4]^-$ ions to 500 μM (pattern g) results in an increase in intensity of the Au (111) peak at 38.0° 2θ, in addition to the appearance of new XRD signatures at 44.5°, 65.0°, and 78.0° 2θ, which correspond to the (200), (220), and (311) crystal planes of fcc Au, respectively. It is notable that up to 500 μM concentration of $[AuBr_4]^-$, the intensity of the peaks attributed to CuTCNQ does not decrease with increasing Au decoration. However, a further increase in $[AuBr_4]^-$ ion concentration to 1 mM, 10 mM, and 100 mM (patterns h, i, and j, respectively) results in more-intense XRD peaks corresponding to fcc Au, and a concomitant reduction in the intensity of the peaks attributed to CuTCNQ is observed. By examining the SEM images corresponding to these sample (Figures 2f–h, respectively), this decrease in CuTCNQ XRD signatures can be attributed to an almost-complete coverage of the CuTCNQ rods by Au clusters in these samples, such that the majority of the X-rays are diffracted by the Au clusters. A relatively higher intensity of the Au (200) peak over the (111) peak is also notable, which suggests the formation of Au nanoparticles of cubic morphology,[52−54] as observed under SEM (see Figures 2e–h and Figures S1e–h in the Supporting Information). In addition, at ion concentrations of 10 mM and 100 mM $[AuBr_4]^-$ (patterns i and j), XRD signatures at 27.0°, 45.1°, 51.2°, and 73.2° 2θ are observed, which correspond to $CuBr_2$ (JCPDS File Card 00-045-1063), as indicated from SEM, EDX, and XPS measurements. A range of additional XRD features in 100 mM sample can be attributed to the formation of a copper bromide hydroxide species $Cu_2Br(OH)_3$ (JCPDS card 00-045-1309), which is not unexpected within an aqueous environment.

4. MECHANISM OF GALVANIC REPLACEMENT

The mechanism of galvanic replacement reaction between CuTCNQ microrods and $[AuBr_4]^-$ ions in water is proposed in Scheme 1. Unlike our previous work concerning the galvanic replacement of CuTCNQ with $[AuBr_4]^-$ ions in acetonitrile,[19] the galvanic replacement of CuTCNQ with $[AuBr_4]^-$ ions in aqueous solution appears to be significantly different, because water does not cause any detectable dissolution of CuTCNQ in the current study. We propose that step 1 involves a redox reaction, akin to the electroless galvanic replacement process, through which $[AuBr_4]^-$ ions are reduced to form metallic Au^0 on the surface of the CuTCNQ rods, while CuTCNQ is simultaneously oxidized to form $TCNQ^0$ and Cu^+ ions via eq 1:

$$2K^+[AuBr_4]^-_{(aq)} + 6CuTCNQ_{(s)} \rightarrow 2Au^0_{(s)} + 6TCNQ^0_{(s)} + 6Cu^+_{(aq)} + 6Br^-_{(aq)} + 2KBr_{(aq)} \quad (1)$$

It has been demonstrated by Bond et al.[50] that CuTCNQ oxidizes over a potential range of 0.5−0.7 V (vs SHE), whereas the standard reduction potential for the $[AuBr_4]^-/Au$ couple is 0.854 V (vs SHE),[55] which provides enough driving force for this reaction to be thermodynamically possible. Also, the

dx.doi.org/10.1021/ic300555j | Inorg. Chem. 2012, 51, 8791−8801

Scheme 2. Schematic Representation of the Galvanic Replacement Reaction between CuTCNQ Microrods and $[AuBr_4]^-$ Ions in the Absence of an Underlying Cu Substrate in an Aqueous Environment[a]

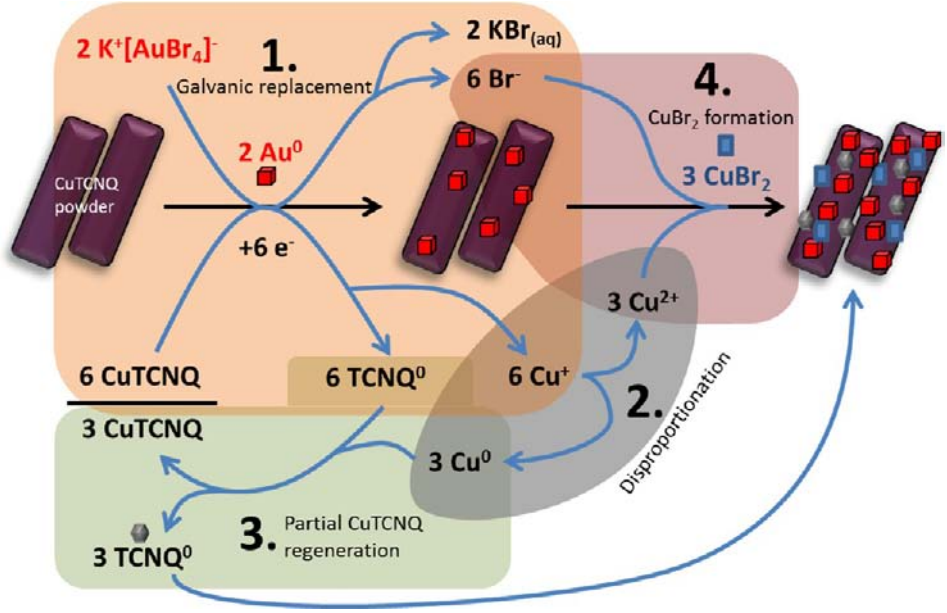

[a]Step 1 involves the galvanic replacement of CuTCNQ by $[AuBr_4]^-$ ions to generate metallic Au^0 by oxidizing CuTCNQ to Cu^+ and $TCNQ^0$, followed by the disproportionation of Cu^+ in water to form Cu^0 and Cu^{2+} (Step 2). Step 3 describes the regeneration of CuTCNQ through reaction between the newly generated Cu^0 and the $TCNQ^0$ that was oxidized from CuTCNQ, notably however, not enough Cu^0 is generated to completely regenerate the oxidized CuTCNQ and as a result residual $TCNQ^0$ remains on the surface of the microrods. Finally, step 4 illustrates the formation of $CuBr_2$ from residual Cu^{2+} and Br^- ions.

possibility of $[AuBr_4]^-$ ions reacting with Cu^+ ions that are liberated during CuTCNQ oxidation can be discounted as Cu^+ ions are unstable in aqueous solutions. Notably, Cu^+ ions formed during galvanic replacement process spontaneously disproportionate to form equal parts Cu^0 and Cu^{2+}, as depicted in step 2 (Scheme 1) and described by eq 2:

$$2Cu^+ \rightarrow Cu^0 + Cu^{2+} \quad (2)$$

While it is true that a redox reaction between Cu^+ and $[AuBr_4]^-$ is thermodynamically possible (where the Cu^+/Cu^{2+} couple is +0.159 V vs SHE), the spontaneous nature of the above-mentioned disproportionation reaction suggests a relatively low percentage of Cu^+ ions are available to react with $[AuBr_4]^-$ ions, therefore having a negligible impact on the mechanism being proposed.

Therefore, in this particular case:

$$6Cu^+_{(aq)} \rightarrow 3Cu^0_{(s)} + 3Cu^{2+}_{(aq)} \quad (3)$$

Furthermore, the Cu^0 species generated through this disproportionation reaction can spontaneously react with the $TCNQ^0$ produced during galvanic replacement of CuTCNQ with $[AuBr_4]^-$ ions (via eq 1) to regenerate half of the CuTCNQ that was originally oxidized as a direct result of galvanic replacement.[56] In order to balance the process and fully utilize the remaining half of $TCNQ^0$ produced during galvanic replacement, the regeneration of all the oxidized CuTCNQ must employ half of the Cu^0 atoms from the underlying Cu substrate via eq 4, as shown in step 3 (Scheme 1):

$$3Cu^0_{(s)} + 3Cu^0_{(\text{from substrate})} + 6TCNQ^0_{(s)} \rightarrow 6CuTCNQ_{(s)} \quad (4)$$

The absence of Raman signatures corresponding to $TCNQ^0$ (Figure 6) during the galvanic replacement reaction between CuTCNQ and $[AuBr_4]^-$ ions in water also supports that the $TCNQ^0$ generated as a result of $[AuBr_4]^-$ reduction via eq 1 must have returned to its original $TCNQ^-$ state (as Cu^+TCNQ^-) via the above reaction denoted in eq 4. This complete regeneration of CuTCNQ explains the observation that CuTCNQ microrods do not undergo any significant size or morphology changes during the galvanic replacement process (Figure 2). However, profile view SEM images (Figure S2 in the Supporting Information) of the galvanically replaced substrates (CuTCNQ on Cu film) demonstrate that the Cu substrate becomes significantly roughened after galvanic replacement with increasing concentration of $[AuBr_4]^-$, thereby further supporting the role of the underlying Cu substrate toward regenerating CuTCNQ during the galvanic replacement process.

Finally, as indicated through step 4 (Scheme 1), the Cu^{2+} ions generated through the disproportionation of Cu^+ (eq 3) are able to diffuse through the solution and react with Br^- ions liberated during the galvanic replacement process (eq 1) to form $CuBr_2$ via eq 5, which precipitates onto CuTCNQ microrods, as was observed for galvanic replacement at higher gold salt concentrations:

$$3Cu^{2+}_{(aq)} + 6Br^-_{(aq)} \rightarrow 3CuBr_{2(s)} \quad (5)$$

Since all the CuTCNQ consumed during galvanic replacement reaction with $[AuBr_4]^-$ is regenerated by utilizing Cu^0 present in the Cu substrate, the concentration of $[AuBr_4]^-$ ions becomes the limiting factor to control the degree of Au loading on CuTCNQ microrods, and as a result, the galvanic replacement process continues until all the $[AuBr_4]^-$ ions have been consumed. Therefore, the overall process of galvanic

dx.doi.org/10.1021/ic300555j | Inorg. Chem. 2012, 51, 8791−8801

replacement between CuTCNQ microrods deposited on a Cu substrate and $KAuBr_4$ in aqueous solution can be described by eq 6:

$$2KAuBr_{4(aq)} + 6CuTCNQ_{(s)} + 3Cu_{(substrate)} \rightarrow 6CuTCNQ/2Au^0_{(s)} + 2KBr_{(s)} + 3CuBr_{2(s)} \quad (6)$$

It must however be noted that, at lower concentrations of $[AuBr_4]^-$ ions, $CuBr_2$ is either not detected or is detected in minuscule amounts at the surface of CuTCNQ/Au nanocomposites. This is most likely due to the diffusion of Cu^{2+} and Br^- ions away from the CuTCNQ surface and the high solubility of $CuBr_2$ (55.7 g/100 mL) which is subsequently removed through washing of the substrate. In addition, the formation of cuprous oxybromide ($Cu_2Br(OH)_3$) species is unlikely because it is completely insoluble in water and would have been detected at the surface of CuTCNQ/Au when the lower concentrations of $KAuBr_4$ were used.[57] This is also supported by the fact that the pH of the solutions were found to be between 7.4 and 7.8. The presence of $CuBr_2$ is also evident from a photograph of the reaction medium after galvanic replacement of substrate with 1 mM $[AuBr_4]^-$ ions, followed by removal of the substrate, which shows a strong greenish-blue precipitate. Corresponding XRD pattern of the precipitated material shows characteristic peaks of $CuBr_2$ (see Figure S3 in the Supporting Information), thus further supporting the proposed reaction mechanism.

A control experiment wherein galvanic replacement of powdered CuTCNQ in the absence of an underlying Cu substrate was investigated as the above proposed mechanism is based on the hypothesis involving the participation of the underlying Cu substrate to enable regeneration of all CuTCNQ oxidized during a galvanic replacement process. In addition, this control experiment also aids in discounting the formation of pinholes in the CuTCNQ, which might expose the underlying Cu substrate to direct oxidation by $[AuBr_4]^-$ ions. Of great consequence, the Raman spectroscopy analysis of the three concentrations of $[AuBr_4]^-$ studied (shown in Figure S4 in the Supporting Information) reveals the formation of neutral $TCNQ^0$ during galvanic replacement in the absence of the Cu substrate, which is not observed when a Cu substrate is present during galvanic replacement (Figure 6). The reaction mechanism in the absence of underlying Cu substrate is demonstrated in Scheme 2. While very similar to Scheme 1 in that steps 1, 2, and 4 are identical, step 3 involving the regeneration of CuTCNQ from $TCNQ^0$ and the Cu^0 species generated through disproportionation of Cu^+ ions cannot completely regenerate all the CuTCNQ oxidized during galvanic replacement. As a result, the residual $TCNQ^0$ remains on the surface of CuTCNQ microrods, which is evident from Raman spectra shown in Figure S4 in the Supporting Information and is described by eq 7:

$$3Cu^0_{(s)} + 6TCNQ^0_{(s)} \rightarrow 3CuTCNQ_{(s)} + 3TCNQ^0_{(s)} \quad (7)$$

Therefore, the overall galvanic replacement process between CuTCNQ powder (i.e., CuTCNQ in the absence of an underlying Cu substrate) and $KAuBr_4$ in aqueous solution can be described by eq 8:

$$2KAuBr_{4(aq)} + 6CuTCNQ_{(s)} \rightarrow 3CuTCNQ/2Au^0_{(s)} + 3TCNQ^0_{(s)} + 2KBr_{(s)} + 3CuBr_{2(s)} \quad (8)$$

The SEM images corresponding to galvanic replacement in the absence of underlying Cu substrate are shown in Figure S5 in the Supporting Information, which demonstrate the decoration of CuTCNQ crystals with increasing density of Au nanoparticles with a corresponding increase in gold salt concentration. As a result of these observations, the participation of the underlying Cu substrate in the regeneration of CuTCNQ after oxidation with $[AuBr_4]^-$ ions can be strongly supported.

5. PHOTOCATALYSIS

It is well-established that surface modification of semiconducting materials such as TiO_2 through decoration of metal nanoparticles can have a positive effect on the photocatalytic properties of the material by enhancing interfacial charge transport and charge separation under band-gap excitation.[28,29,58,59] A schematic representation of a plausible mechanism involved in photocatalysis activity of semiconducting CuTCNQ decorated with metal nanoparticles is shown in Scheme 3. An incident photon of sufficient energy

Scheme 3. Schematic Representation of a Potential Photocatalysis Mechanism for the Synthesized CuTCNQ/Au Nanocomposites[a]

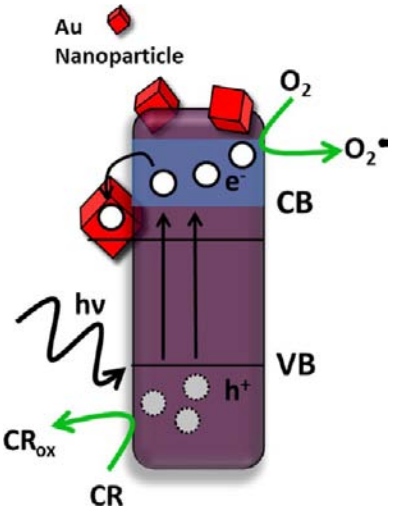

[a]CR and CR_{ox} correspond to the Congo red dye before and after its oxidation, respectively; hν represents an incident photon and VB and CB represent the valence band and the conduction band of the semiconducting CuTCNQ, respectively.

can interact with electrons in the valence band (VB) of CuTCNQ and promote them across the band gap to the conduction band (CB), where there exists a very large driving force to recombine the electron (e^-) and newly generated positive hole (h^+) known as the electron/hole recombination phenomenon.[60] However, by depositing metal nanoparticles on the surface of the semiconductor, Schottky barriers can be formed at the junction of metal nanoparticle and semiconductor,[61] because of differences in the Fermi energy levels of the metal and semiconductor.[62] This difference in Fermi

dx.doi.org/10.1021/ic300555j | Inorg. Chem. 2012, 51, 8791−8801

energy levels leads to continuous transfer of electrons from the semiconductor to the metal until equalization of the Fermi energy levels is achieved, resulting in the distribution of electrons between the semiconductor and metal nanoparticles. This transfer of electrons can help to significantly suppress the electron/hole recombination phenomenon through trapping of electrons behind the Schottky barrier. The positive holes are then able to diffuse to the surface of the semiconductor and facilitate the oxidation of Congo red in solution; in addition, electrons are able to react with oxygen molecules dissolved in solution to form the superoxide radical ($O_2^{\bullet}$) which can then also react with the Congo red dye.[60] Significantly, because the metal nanoparticles in this nanocomposite act as an effective means of suppressing the electron/hole recombination phenomenon, the photocatalytic performance of the nanocomposite should be appreciably tunable with the degree of loading and composition of metal on the surface.[63] We recently demonstrated for the first time that phase I CuTCNQ-based materials can be appreciably employed for photocatalytic activities.[19] Therefore, the CuTCNQ/Au nanocomposites prepared in this study via galvanic replacement in water were explored for their photocatalytic activity against a model azo dye (Congo red). Figure 8 shows the photodegradation

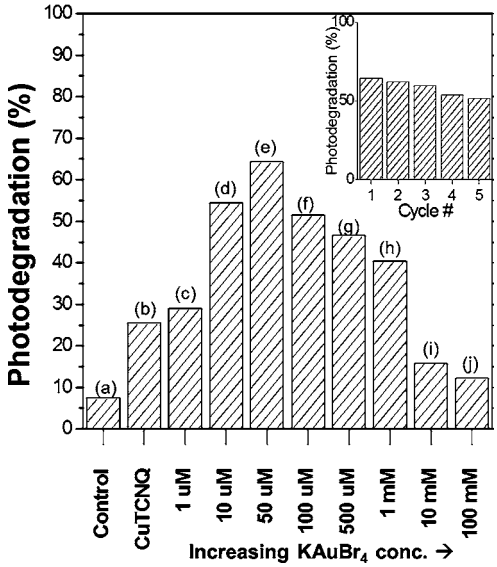

Figure 8. Percentage photodegradation of 50 μM aqueous solution of the organic dye Congo red under simulated solar light conditions for 30 min as recorded by UV−vis spectroscopy by measuring dye absorbance maxima at 500 nm: (a) Congo red control, (b) pristine CuTCNQ, and CuTCNQ reacted with (c) 1 μM, (d) 10 μM, (e) 50 μM, (f) 100 μM, (g) 500 μM, (h) 1 mM, (i) 10 mM, and (j) 100 mM $[AuBr_4]^-$ ions. The inset shows the percentage photodegradation of 50 μM aqueous solution of the organic dye Congo red under simulated solar light conditions for 30 min by the CuTCNQ sample reacted with 50 μM $[AuBr_4]^-$ over multiple cycles.

efficiency of CuTCNQ substrates prepared before and after galvanic replacement with increasing concentrations of $[AuBr_4]^-$ ions in aqueous solution by irradiating 50 μM Congo red aqueous solutions for 30 min under simulated solar light (equator conditions). In the absence of a CuTCNQ catalyst (column a in Figure 8), the solar radiation causes ca. 7% of the dye to degrade, which, upon introduction of a pristine phase I CuTCNQ substrate, increases to ca. 26%, thereby indicating that phase I CuTCNQ without modification has a slight degree of photocatalytic activity. When the phase I CuTCNQ substrates are galvanically replaced with increasing concentrations of $[AuBr_4]^-$ ions in aqueous solution, the photocatalytic activity is initially observed to increase to 29% for 1 μM $[AuBr_4]^-$ ions (column c in Figure 8) and 54% for 10 μM $[AuBr_4]^-$ ions (column d in Figure 8), before reaching a maximum of ca. 64% degradation at galvanic replacement with 50 μM $[AuBr_4]^-$ ions (column e in Figure 8). Our group and others have previously shown that the extent of metal loading on semiconductor photocatalyst surfaces such as TiO_2 is directly related to the photocatalytic performance of the material, and above an optimum loading level, the efficiency is observed to decrease.[29,60] Our observations suggest that the semiconductor charge transfer complexes of CuTCNQ seem to behave in a similar fashion, wherein galvanic replacement with 100 μM $[AuBr_4]^-$ ions (column f in Figure 8) results in a decrease in photocatalytic efficiency to 51%, because of a greater loading of Au nanoparticles on the CuTCNQ surface. Further increasing the $[AuBr_4]^-$ ion concentration to 500 μM (column g in Figure 8) and 1 mM (column h in Figure 8) results in further decrease in photodegradation of organic dye, leading to 46% and 40% degradation, respectively. Interestingly, further increasing the $[AuBr_4]^-$ ion concentration to 10 mM and 100 mM (see columns i and j, respectively, in Figure 8) causes the observed degradation of Congo red to fall to 16% and 12%, respectively, which is even lower than that observed for pristine phase I CuTCNQ. This dramatic decrease at significantly high gold salt concentrations can be attributed to the remarkably high degree of metal loading on the CuTCNQ surface, as observed under SEM (Figures 2g and 2h), which, in turn, does not allow incident photons to interact with the underlying CuTCNQ material. To demonstrate the reusability of the CuTCNQ/Au nanocomposites, the photocatalytic activity of CuTCNQ reacted with 50 μM $[AuBr_4]^-$ ions (which demonstrated the highest photocatalytic activity in the previous experiment) was studied over five cycles. Shown in the inset of Figure 8, the photocatalytic activity of this nanocomposite is observed to decrease slightly with repeated photocatalytic experiments; however, even after five cycles, the decrease in photocatalytic activity is only ca. 10%, demonstrating both significant stability and reusability.

6. CONCLUSIONS

This study has investigated the spontaneous galvanic replacement of semiconducting charge transfer complex of phase I CuTCNQ with $[AuBr_4]^-$ ions in an aqueous environment, which leads to tunable decoration of CuTCNQ microrods with metallic Au nanoparticles by controlling the concentration of gold ions during the reaction. The study reveals an interesting mechanism of galvanic replacement of CuTCNQ with $[AuBr_4]^-$ ions in water, wherein CuTCNQ crystals oxidized by $[AuBr_4]^-$ ions during galvanic replacement process were found to be completely regenerated partly due to a Cu^+ ion disproportionation mechanism, and in part, due to the mechanism involving the underlying Cu substrate. The reaction mechanism observed here in water is significantly different in comparison with our previous study in acetonitrile under similar conditions, wherein it was established that the underlying Cu substrate on which CuTCNQ microrods are grown, does not participate during galvanic replacement reaction, and that the reaction in acetonitrile proceeds via two competing reaction mechanisms involving dissolution of CuTCNQ in acetonitrile and galvanic replacement. Also, since

dx.doi.org/10.1021/ic300555j | Inorg. Chem. 2012, 51, 8791−8801

Cu^+ ions are stable in acetonitrile (in contrast to the current study in water), the disproportionation of Cu^+ ions does not take place in acetonitrile, leading to a completely different reaction mechanism in these two solvents. Therefore, the current work highlights the importance of the choice of an appropriate solvent during galvanic replacement reactions, which can have significant impact on the reaction outcomes.[32] Furthermore, the galvanic replacement approach of Au nanoparticle decoration onto CuTCNQ reported in this work opens up new possibilities of studying other metal-TCNQ organic semiconducting materials that could, in turn, be galvanically replaced with different noble metals such as gold, platinum, and palladium, leading to potentially novel applications in photocatalysis, catalysis and sensing.

■ ASSOCIATED CONTENT

Supporting Information

Additional SEM images and supporting XRD and Raman analysis of CuTCNQ samples galvanically replaced with different concentrations of $[AuBr_4]^-$ ions. This material is available free of charge via the Internet at http://pubs.acs.org.

■ AUTHOR INFORMATION

Corresponding Author

*Tel.: 0061 3 99252121. Fax: 0061 3 99253747. E-mail: vipul.bansal@rmit.edu.au (V.B.); suresh.bhargava@rmit.edu.au (S.K.B.).

Notes

The authors declare no competing financial interest.

■ ACKNOWLEDGMENTS

V.B. thanks the Australian Research Council (ARC) for APD Fellowship and financial support through the ARC Discovery Project (No. DP0988099) and acknowledges the support of the Ian Potter Foundation in establishing a multimode advanced spectroscopy facility at RMIT University. A.O.M. thanks the ARC for financial support through a Future Fellowship (FT110100760). V.B., A.O.M., and S.K.B. thank the ARC for financial support through Linkage Project No. LP100200859 and Discovery Project No. DP110105125.

■ REFERENCES

(1) Heintz, R. A.; Zhao, H.; Ouyang, X.; Grandinetti, G.; Cowen, J.; Dunbar, K. R. *Inorg. Chem.* **1999**, *38*, 144.
(2) Miyasaka, H.; Motokawa, N.; Matsunaga, S.; Yamashita, M.; Sugimoto, K.; Mori, T.; Toyota, N.; Dunbar, K. R. *J. Am. Chem. Soc.* **2010**, *132*, 1532.
(3) Clerac, R.; O'Kane, S.; Cowen, J.; Ouyang, X.; Heintz, R.; Zhao, H.; Bazile, M. J., Jr.; Dunbar, K. R. *Chem. Mater.* **2003**, *15*, 1840.
(4) Wang, X.; Liable-Sands, L. M.; Manson, J. L.; Rheingold, A. L.; Miller, J. S. *Chem. Commun.* **1996**, 1979.
(5) Vickers, E. B.; Selby, T. D.; Thorum, M. S.; Taliaferro, M. L.; Miller, J. S. *Inorg. Chem.* **2004**, *43*, 6414.
(6) Garcia-Yoldi, I.; Miller, J. S.; Novoa, J. J. *J. Phys. Chem. A* **2009**, *113*, 7124.
(7) Neufeld, A. K.; O'Mullane, A. P.; Bond, A. M. *J. Am. Chem. Soc.* **2005**, *127*, 13846.
(8) O'Mullane, A. P.; Neufeld, A. K.; Harris, A. R.; Bond, A. M. *Langmuir* **2006**, *22*, 10499.
(9) Nafady, A.; Bond, A. M.; Bilyk, A.; Harris, A. R.; Bhatt, A. I.; O'Mullane, A. P.; De Marco, R. *J. Am. Chem. Soc.* **2007**, *129*, 2369.
(10) O'Mullane, A. P.; Fay, N.; Nafady, A.; Bond, A. M. *J. Am. Chem. Soc.* **2007**, *129*, 2066.
(11) Nafady, A.; Bond, A. M. *Inorg. Chem.* **2007**, *46*, 4128.
(12) Zhao, C.; MacFarlane, D. R.; Bond, A. M. *J. Am. Chem. Soc.* **2009**, *131*, 16195.
(13) Nafady, A.; Bond, A. M.; O'Mullane, A. P. *Inorg. Chem.* **2009**, *48*, 9258.
(14) Potember, R. S.; Poehler, T. O.; Benson, R. C. *Appl. Phys. Lett.* **1982**, *41*, 548.
(15) Xiao, K.; Ivanov, I. N.; Puretzky, A. A.; Liu, Z.; Geohegan, D. B. *Adv. Mater. (Weinheim, Ger.)* **2006**, *18*, 2184.
(16) Muller, R.; Genoe, J.; Heremans, P. *Appl. Phys. Lett.* **2006**, 88.
(17) Oyamada, T.; Tanaka, H.; Matsushige, K.; Sasabe, H.; Adachi, C. *Appl. Phys. Lett.* **2003**, *83*, 1252.
(18) Liu, H.; Liu, Z.; Qian, X.; Guo, Y.; Cui, S.; Sun, L.; Song, Y.; Li, Y.; Zhu, D. *Cryst. Growth Des.* **2009**, *10*, 237.
(19) Pearson, A.; O'Mullane, A.; Bhargava, S. K.; Bansal, V. *Inorg. Chem. (Washington, DC, U. S.)* **2011**, *50*, 1705.
(20) Muller, R.; De Jonge, S.; Myny, K.; Wouters, D. J.; Genoe, J.; Heremans, P. *Solid-State Electron.* **2006**, *50*, 602.
(21) Duan, H.; Cowan, D. O.; Kruger, J. *Mater. Res. Soc. Symp. Proc.* **1990**, *173*, 165.
(22) Liu, S.-G.; Liu, Y.-Q.; Wu, P.-J.; Zhu, D.-B. *Chem. Mater.* **1996**, *8*, 2779.
(23) Liu, H.; Zhao, Q.; Li, Y.; Liu, Y.; Lu, F.; Zhuang, J.; Wang, S.; Jiang, L.; Zhu, D.; Yu, D.; Chi, L. *J. Am. Chem. Soc.* **2005**, *127*, 1120.
(24) Liu, Y. L.; Ji, Z. Y.; Tang, Q. X.; Jiang, L.; Li, H. X.; He, M.; Hu, W. P.; Zhang, D. Q.; Wang, X. K.; Wang, C.; Liu, Y. Q.; Zhu, D. B. *Adv. Mater. (Weinheim, Ger.)* **2005**, *17*, 2953.
(25) Sharma, S. D.; Saini, K. K.; Kant, C.; Sharma, C. P.; Jain, S. C. *Appl. Catal., B* **2008**, *84*, 233.
(26) Mahmoodi, N. M.; Arami, M.; Limaee, N. Y.; Gharanjig, K. *J. Hazard. Mater.* **2007**, *145*, 65.
(27) Barraud, E.; Bosc, F.; Edwards, D.; Keller, N.; Keller, V. *J. Catal.* **2005**, *235*, 318.
(28) Pearson, A.; Bhargava, S. K.; Bansal, V. *Langmuir* **2011**, *27*, 9245.
(29) Pearson, A.; Jani, H.; Kalantar-Zadeh, K.; Bhargava, S. K.; Bansal, V. *Langmuir* **2011**, *27*, 6661.
(30) Sadek, A.; Zheng, H.; Breedon, M.; Bansal, V.; Bhargava, S. K.; Latham, K.; Zhu, J.; Yu, L.; Hu, Z.; Spizzirri, P. G.; Wlodarski, W.; Kalantar-zadeh, K. *Langmuir* **2009**, *25*, 9545.
(31) Kalantar-zadeh, K.; Sadek, A. Z.; Zheng, H.; Bansal, V.; Bhargava, S. K.; Wlodarski, W.; Zhu, J.; Yu, L.; Hu, Z. *Sens. Actuators, B* **2009**, *142*, 230.
(32) Pearson, A.; O'Mullane, A. P.; Bansal, V.; Bhargava, S. K. *Chem. Commun.* **2010**, *46*, 731.
(33) Cobley, C. M.; Xia, Y. *Mater. Sci. Eng.: R: Rep.* **2010**, *70*, 44.
(34) Lu, X.; Chen, J.; Skrabalak, S. E.; Xia, Y. *Proc. Inst. Mech. Eng., Part N: J. Nanoeng. Nanosyst.* **2007**, *221*, 1.
(35) Xia, Y.; Li, W.; Cobley, C. M.; Chen, J.; Xia, X.; Zhang, Q.; Yang, M.; Cho, E. C.; Brown, P. K. *Acc. Chem. Res.* **2011**, *44*, 914.
(36) Zhang, Q.; Wang, W.; Goebl, J.; Yin, Y. *Nano Today* **2009**, *4*, 494.
(37) Bai, X.; Gao, Y.; Zheng, L. *CrystEngComm* **2011**, *13*, 3562.
(38) Lu, X.; Tuan, H.-Y.; Chen, J.; Li, Z.-Y.; Korgel, B. A.; Xia, Y. *J. Am. Chem. Soc.* **2007**, *129*, 1733.
(39) Kwon, S.; Dong, H.; Lee, S.-Y. *J. Nanomater.* **2010**, *2010*.
(40) Ortiz, N.; Skrabalak, S. E. *Cryst. Growth Des.* **2011**, *11*, 3545.
(41) Zhao, L.; Ding, K.; Ji, X.; Li, J.; Wang, H.; Yang, W. *Colloids Surf., A* **2011**, *386*, 172.
(42) Bansal, V.; O'Mullane, A. P.; Bhargava, S. K. *Electrochem. Commun.* **2009**, *11*, 1639.
(43) Guo, S.; Dong, S.; Wang, E. *Chem.—Eur. J.* **2008**, *14*, 4689.
(44) Chen, Q.-S.; Sun, S.-G.; Zhou, Z.-Y.; Chen, Y.-X.; Deng, S.-B. *Phys. Chem. Chem. Phys.* **2008**, *10*, 3645.
(45) Bansal, V.; Jani, H.; Du Plessis, J.; Coloe, P. J.; Bhargava, S. K. *Adv. Mater. (Weinheim, Ger.)* **2008**, *20*, 717.
(46) Au, L.; Lu, X.; Xia, Y. *Adv. Mater. (Weinheim, Ger.)* **2008**, *20*, 2517.
(47) Bansal, V.; Syed, A.; Bhargava, S. K.; Ahmad, A.; Sastry, M. *Langmuir* **2007**, *23*, 4993.

(48) Yang, M.; Zhu, J.-J.; Li, J.-J. *J. Cryst. Growth* **2004**, *267*, 283.
(49) Joshi, H.; Shirude, P. S.; Bansal, V.; N., G. K.; Sastry, M. *J. Phys. Chem. B* **2004**, *108*, 11535.
(50) Harris, A. R.; Neufeld, A. K.; O'Mullane, A. P.; Bond, A. M.; Morrison, R. J. S. *J. Electrochem. Soc.* **2005**, *152*, C577.
(51) O'Mullane, A. P.; Ippolito, S. J.; Sabri, Y. M.; Bansal, V.; Bhargava, S. K. *Langmuir* **2009**, *25*, 3845.
(52) Plowman, B.; Ippolito, S. J.; Bansal, V.; Sabri, Y. M.; O'Mullane, A. P.; Bhargava, S. K. *Chem. Commun.* **2009**, 5039.
(53) Bansal, V.; Li, V.; O'Mullane, A. P.; Bhargava, S. K. *CrystEngComm* **2010**, *12*, 4280.
(54) Sabri, Y. M.; Ippolito, S. J.; O'Mullane, A. P.; Tardio, J.; Bansal, V.; Bhargava, S. K. *Nanotechnology* 2011, *22*.
(55) Evans, D. H.; Lingane, J. J. *J. Electroanal. Chem.* **1963**, *6*, 1.
(56) Neufeld, A. K.; Madsen, I.; Bond, A. M.; Hogan, C. F. *Chem. Mater.* **2003**, *15*, 3573.
(57) Richards, T. W. *Proc. Am. Acad. Arts Sci.* **1889**, *25*, 215.
(58) Dawson, A.; Kamat, P. V. *J. Phys. Chem. B* **2001**, *105*, 960.
(59) Jakob, M.; Levanon, H.; Kamat, P. V. *Nano Lett.* **2003**, *3*, 353.
(60) Linsebigler, A. L.; Lu, G.; Yates, J. T. *Chem. Rev.* **1995**, *95*, 735.
(61) Iliev, V.; Tomova, D.; Bilyarska, G.; Tyuliev, G. *J. Mol. Catal. A: Chem.* **2007**, 32.
(62) Kamat, P. V. *J. Phys. Chem. B* **2002**, *106*, 7729.
(63) Jakob, M.; Levanon, H.; Kamat, P. V. *Nano Lett.* **2003**, *3*, 353.